ACS APPLIED MATERIALS & INTERFACES

Research Article

www.acsami.org

Bacterial Cellulose Supported Gold Nanoparticles with Excellent Catalytic Properties

Meiyan Chen,[†,‡] Hongliang Kang,[*,‡] Yumei Gong,[*,†] Jing Guo,[†] Hong Zhang,[†] and Ruigang Liu[*,‡]

[†]School of Textile and Material Engineering, Dalian Polytechnic University, Dalian, 116034, China

[‡]Sate Key Laboratory of Polymer Physics and Chemistry, Beijing National Laboratory of Molecular Sciences, Institute of Chemistry, Chinese Academy of Sciences, Beijing 100190, China

Supporting Information

ABSTRACT: Amidoxime surface functionalized bacterial cellulose (AOBC) has been successfully prepared by a simple two-step method without obviously changing the morphology of bacterial cellulose. AOBC has been used as the reducing agent and carrier for the synthesis of gold nanoparticles (AuNPs) that distributed homogeneously on bacterial cellulose surface. Higher content in amidoxime groups in AOBC is beneficial for the synthesis of AuNPs with smaller and more uniform size. The AuNPs/AOBC nanohybrids have excellent catalytic activity for reduction of 4-nitrophenol (4-NP) by using $NaBH_4$. It was found that catalytic activity of AuNPs/AOBC first increases with increasing $NaBH_4$ concentration and temperature, and then leveled off at $NaBH_4$ concentration above 238 mM and temperature above 50 °C. Moreover, AuNPs with smaller size have higher catalytic activity. The highest apparent turnover frequency of AuNPs/AOBC is 1190 h^{-1}. The high catalytic activity is due to the high affinity of 4-NP with AuNPs/AOBC and the reduced product 4-aminophenol has good solubility in water in the presence of AuNPs/AOBC. The catalytic stability of the AuNPs/AOBC was estimated by filling a fluid column contained AuNPs/AOBC and used for continuously catalysis of the reduction of 4-NP by using $NaBH_4$. The column works well without detection of 4-NP in the eluent after running for more than two months, and it is still running. This work provides an excellent catalyst based on bacterial cellulose stabilized AuNPs and has promising applications in industry.

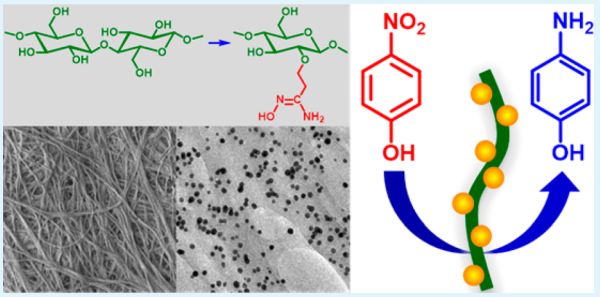

KEYWORDS: *bacterial cellulose, surface modification, gold nanoparticles, amidoxime, nanohybrids, catalysis, reducing reaction*

INTRODUCTION

Gold nanoparticles (AuNPs) have attracted increasing interest for their fascinating optical, electronic, and chemical properties,[1−3] which offer promising applications in many fields such as catalysis.[4−7] The catalytic activity of AuNPs definitely depends on their size, shape, and surface functionality. A great deal of effort has been directed toward controlling the size and shape of AuNPs in the literature.[8−12] However, direct introduction of AuNPs into reaction systems tends to lead to aggregation due to the large specific surface area. On the other hand, separation and recovery of AuNPs from the reaction solution media are commonly difficult. Therefore, AuNPs are better loaded in polymer matrix[13,14] or porous inorganic materials[15,16] to prevent their aggregation. Polymeric supports are attractive due to a greater number of active sites and designation in the structure and function.[17,18] Using polymers as the support for AuNPs is beneficial for controlling particle growth as well as stabilizing the resulting AuNPs.

Eco-friendly polymers from renewable resources have been used as AuNP supports for their biodegradability and biocompatibility.[19−21] As the most abundant natural polymer, cellulose can be easily chemically modified through the hydroxyl groups.[22,23] Many efforts have been devoted to the deposition of AuNPs on cellulose matrix. Huang et al.[24] fabricated a AuNPs-containing cellulose membrane by introduction of AuNPs onto cellulose fibers precoated with titania gel. However, this approach was rather complicated and 5-cycle deposition of titania gel was performed first, and then positively and negatively charged polymers and $KAuCl_4$ were alternatively deposited on the titania gel film many times. The film was finally treated with $NaBH_4$ aqueous solution to reduce $AuCl_4^-$ into AuNPs. Moreover, poly(ethylenimine) (PEI)[25] and poly(diallyldimethylammonium chloride) (PDDA)[26] were coated onto the surface of the cellulose matrix to enhance the interaction between cellulose and AuNPs. Some researchers reported directly deposited AuNPs obtained from reducing products by $NaBH_4$ on the surface of modified cellulosic substrates with functional groups, e.g., −HS,[27] −COOH,[28] or $-NH_3^+$.[29] He et al. utilized the porous structure in cellulose to adsorb $AuCl_4^-$ ions and then reduced in $NaBH_4$ aqueous solution to prepared AuNPs with the size less than 10 nm.[30,31] Most approaches in the literature can prepare AuNPs with

Received: May 20, 2015
Accepted: September 11, 2015
Published: September 11, 2015

DOI: 10.1021/acsami.5b07150
ACS Appl. Mater. Interfaces 2015, 7, 21717−21726

small size, but toxic or dangerous reducing agents such as $NaBH_4$ are generally used and the resultant AuNPs must be stabilized by further surface modification.[32] For pursuing an eco-friendly process, synthesis of AuNPs *in situ* on paper sheets was achieved without using a reducing agent.[33] AuNPs were synthesized on a cellulose matrix by a hydrothermal method, in which hydroxyl groups of cellulose were used as the reducing agent, but the size of AuNPs was usually not controllable and adjustable.[19] In our previous work, carboxymethyl cellulose (CMC) was used as both the reducing and stabilizing agent for preparing AuNPs. However, irreversible aggregation of AuNPs occurred at low pH and cysteamine was needed to costabilize AuNPs with CMC in aqueous solution.[20] In the green approach of preparing AuNPs, considering easy aggregation of these particles, it is necessary to strengthen the interactions between cellulose and AuNPs, which still remains a challenge.[34]

AuNPs loaded on cellulose have been used as the catalysts in reducing 4-nitrophenol. AuNPs loaded on nanocellulose showed a relatively lower catalytic reaction rate $k = 2.06 \times 10^{-3}$ s^{-1} and apparent turnover frequency (TOF_a) of 109 h^{-1}, which could be due to the uncontrollable size of AuNPs.[19] AuNPs loaded on coated PEI showed good catalytic activity with catalytic reaction rate of $k = 5.1 \times 10^{-3}$ s^{-1} and TOF_a of 212 h^{-1}.[25] The AuNPs loaded on cellulose single nanofibers using carboxylate groups as selective sites have $k = 5.9 \times 10^{-3}$ s^{-1} and TOF_a of 563 h^{-1}.[28]AuNPs deposited on the PDDA surface-coated carboxylated nanocrystalline cellulose have $k = 4.4 \times 10^{-3}$ s^{-1} and TOF_a of 540 h^{-1}.[26] However, the catalytic activity of AuNPs supported by cellulose is still lower than that of AuNPs supported by inorganic materials.[35] Moreover, it still remains a challenge to promote the catalytic activity[35] and to overcome the rapid loss of catalytic efficiency due to the aggregation of cellulose supported AuNPs. We have proven that the introduction of amidoxime groups on cellulose backbones can excellently stabilize AuNPs on cellulose.[21] The amidoxime group contains hydroxyimino and amino groups, which offer the fused features of amide, oxime, amidine, and hydroxamic acid, and has strong chelation ability for metal ions, which prevent the precipitation of metal nanoparticles.[21,36]

Bacteria cellulose (BC) contains highly crystalline ultrafine nanofibers with width less than 100 nm and abundance in hydroxyl groups on surfaces to be functionalized.[37−40] Moreover, the higher tensile strength[19,20] and lower axial thermal expansion coefficient[41] of BC are good for applications in various fields. In this work, amidoxime groups were first introduced on the surface of BC nanofibers (AOBC) to enhance the interaction between BC and AuNPs. AuNPs were synthesized *in situ* on the BC surface by a one-step hydrothermal process in $HAuCl_4$ aqueous solution by using AOBC as both reducing and stabilizing agents. The catalytic activity and stability of AOBC-loaded AuNPs were checked by catalyzing the reduction of 4-nitrophenol (4-NP) using $NaHB_4$ as the model reaction. We found that the AOBC-loaded AuNPs have the excellent catalytic activity and stability. The effects of temperature, the content of reducing agent, and AuNP size on the catalytic activity were also investigated in detail.

EXPERIMENTAL SECTION

Materials. Bacterial cellulose (BC), a product of *Gluconacetobacter xylinum*, was milled using a Supermasscolloider (Mini MKCA6−2) to result in a BC nanofibril suspension with BC content of 0.9 wt %, which was stored at 4 °C before use. Hydroxylamine hydrochloride ($NH_2OH·HCl$, 99.9%, Alfa Aesar), acrylonitrile (CH_2CHCN, 98%, Beijing Chem. Plant), NaOH (≥96%, Sinopharm Chem. Reagent Co. Ltd.), chloroauric acid ($HAuCl_4·4H_2O$, 47.8 wt % Au, Jinke Reagent Factory), $NaBH_4$ (≥97%, Sinopharm Chem. Reagent Co. Ltd.), and 4-nitrophenol (4-NP, ≥99%, Alfa Aesar) were used as received. Water from Milli-Q Reference Water Purification System (Millipore) was used.

Synthesis of Amidoxime Bacterial Cellulose. The amidoxime surface functionalized bacterial cellulose (AOBC) was synthesized by a two-step approach (Scheme 1). Typically, BC (0.36 g) was dispersed in 40 mL NaOH solution (1 mol/L) and stored at room temperature for 7 h for activation, and then acrylonitrile (0.30 mol, 20 mL) was added dropwise under stirring. The reaction was performed at room temperature for 12 h, then BC was separated from the reaction mixture by centrifugation and washed with water several times to remove all soluble components to obtain cyanoethyl surface functionalized bacterial cellulose (CEBC). CEBC was then dispersed in $NaOH/NH_2OH·HCl$ (1:1, mole ratio) aqueous solution (50 mL) and stirred for 10 h at 50 °C, during which the cyano groups changed into amidoxime groups to result in AOBC. AOBC was separated from the reaction mixture by centrifugation, washed with water to remove all the soluble components, and freeze−dried. AOBC with the content of amidoxime groups of 13.6, 14.5, 15.9, and 16.8 wt %, which was estimated by the elemental analysis, were used for the preparation of AuNPs.

Scheme 1. Surface Amidoxime Modification of Bacterial Cellulose

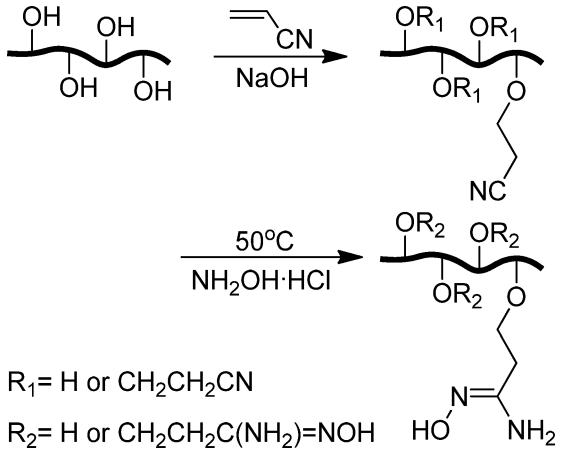

Preparation of AuNPs/AOBC Nanohybrids. AOBC (0.06 g) was dispersed in 10 mL water and then 30 μL of $HAuCl_4$ aqueous solution (0.05 M) was added. The reaction vessel was then sealed and transferred to an oil bath of 110 °C (the pressure in the vessel is about 143 kPa). The reaction was performed with continuously stirring at 110 °C for 2 h, during which the reaction mixture changed from light yellow to pink purple. The reaction mixture was separated by centrifugation. The precipitate was obtained by removing supernatant and washed with water to result in AuNPs/AOBC.

Catalytic Activity of AuNPs/AOBC. The reduction of 4-NP by $NaBH_4$ was used as a model reaction to check the catalytic activity of AuNPs/AOBC. Typically, AuNPs/AOBC aqueous suspension (1 mL) was added into a mixed aqueous solution of 50 mL containing 4-NP (0.30 mM) and $NaBH_4$ (264 mM) under stirring at room temperature (25 °C). The content of AuNPs in the mixture was 0.0286 mg/mL in all experiments. The reduction process was monitored by recording the UV−vis spectra of the reaction mixture at 2 min intervals during the reaction. The reaction rate constant was determined by measuring the absorbance intensity of the initially observed peak at 400 nm, from the nitrophenolate ion, as a function of time. The effects of $NaBH_4$ concentration or temperature on the catalytic activity for the reduction were also investigated by varying the $NaBH_4$ concentration or temperature of the reaction system with the other parameters kept the same. For checking the influence of the AuNPs size on the catalytic

DOI: 10.1021/acsami.5b07150
ACS Appl. Mater. Interfaces 2015, 7, 21717−21726

activity, the concentrations of 4-NP, $NaBH_4$, and AuNPs in all reaction mixtures were kept at 0.30 mM, 264 mM, and 0.0106 mg/mL, respectively, under 25 °C.

Characterization and Measurements. Fourier transform infrared spectra (FTIR) were recorded on a Bruker-Equinox 55 FT-IR spectrometer using KBr pellet. Each spectrum was obtained by 32 scans from 4000 to 400 cm^{-1} at a resolution of 4 cm^{-1}. UV−vis spectra were recorded on a Shimadzu UV-1601 PC spectrophotometer. Scanning electron microscopy (SEM) observation was carried out on a field emission scanning electron microscope (JEOL 6700, Japan) operated at accelerating voltage of 5 kV and current of 10 μA. Transmission electron microscopy (TEM) observation was carried out on a transmission electron microscope (2200FS, JEOL, Japan) operated at 200 kV. The size of AuNPs was determined from TEM images by using Image-J software. X-ray diffraction (XRD) patterns were collected using a Rigaku Analytical X'Pert X-diffractometer (Rigaku, Japan), with Cu K_α radiation (λ = 0.154 nm) at an accelerating voltage of 40 kV and a current of 200 mA. The data were collected from 5° to 90° with a step interval of 0.02°.

Specific surface area of AuNPs/AOBC was measured on a surface area and porosity analyzer (Micromeretics Ltd., ASAP 2020 HD88) according Brunauer−Emmett−Teller (BET) method. ^{1}H NMR measurements were carried out with a Bruker DMX 400 NMR instrument (^{1}H NMR frequency = 400.13 MHz) using D_2O as the solvent. The content of Au in the samples was measured by using inductively coupled plasma (ICP) analysis on an Inductively Coupled Plasma Optical Emission Spectrometer (ICP-OES, iCAP-6300, Thermo Fisher Scientific). Elemental analysis (CHN) was performed on a Flash EA 1112 elemental analyzer.

RESULTS AND DISCUSSION

Synthesis of AOBC. Figure 1 shows the typical SEM images of BC and AOBC nanofibers. The BC nanofibers have

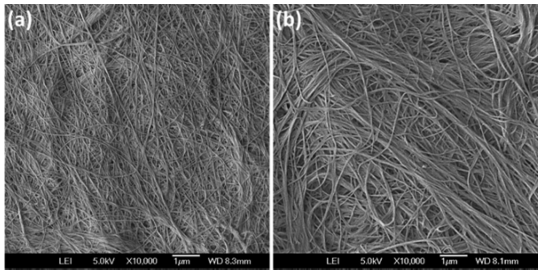

Figure 1. SEM images of (a) BC and (b) AOBC with the amidoxime group content of 16.8 wt %.

diameter of about 30 nm with length of tens of micrometers after grinding (Figure 1a). After surface modification by amidoxime groups, AOBC has similar morphology to that of BC (Figure 1b). The hydroxyl groups on BC nanofibers can be activated under alkaline conditions, which can promote a Michael addition reaction of the hydroxyl groups on BC nanofiber surface with acrylonitrile.[19] The activation conditions and corresponding results of CEBC synthesis are listed in Table S1. All the BC nanofibers (0.36 g) were treated in 40 mL NaOH aqueous solution with different NaOH content, and then desired amounts of acrylonitrile were added in the reaction mixture. The results show that the content of cyano groups in CEBC increases with the activation time and reaches the highest value of 27.4% at the activation time of 7 h. A further increase in activation time leads to a decrease in the content of cyano groups in the resultant CEBC. Therefore, the activation time was selected as 7 h for the synthesis of CEBC. The conversion of cyano groups into amidoxime groups was achieved by treating CEBC with $NH_2OH{\cdot}HCl$ (Scheme 1). Generally, the conversion of cyano groups into amidoxime groups depends on the feeding hydroxylamine hydrochloride with the other parameters kept the same. In this work, excess $NH_2OH{\cdot}HCl$ was used to ensure complete conversion of cyano groups into amidoxime groups.

The typical FTIR spectra of CEBC and AOBC are shown in Figure 2. The sharp band at 2252 cm^{-1} on the spectrum comes

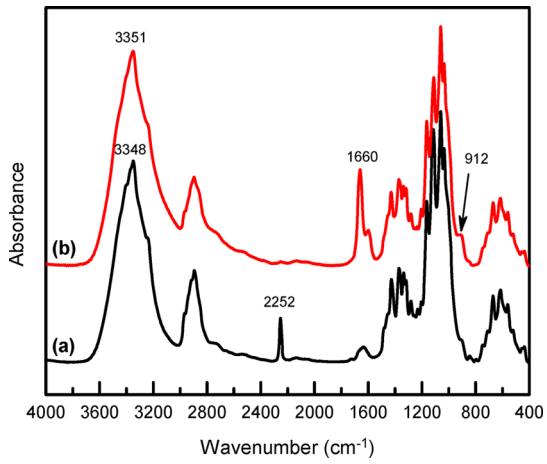

Figure 2. Typical FT-IR spectra of (a) CEBC and (b) AOBC with the amidoxime group content of 16.8 wt %.

from the stretching vibration of —C≡N on the spectrum of CEBC (Figure 2a), which confirms the success of the surface modification of BC nanofibers with ethyl cyano groups via Michael addition. After treatment with $NH_2OH{\cdot}HCl$/NaOH aqueous solution, the characteristic absorbance band of —C≡N at 2252 cm^{-1} disappears and new absorbance bands at 1660 and 912 cm^{-1} appear on the FTIR spectrum of AOBC (Figure 2b), attributing to the stretching vibration of —C═N and —N−OH, respectively.[21,39] Moreover, the band at around 3348 cm^{-1} of the stretching vibration of −OH in the FTIR spectrum of CEBC (Figure 2a) shifts to around 3351 cm^{-1} and becomes broader than that of AOBC (Figure 2b), which is due to the presence of $-NH_2$ groups in AOBC.[39] FTIR results confirm that cyano groups in CEBC have been completely converted into amidoxime groups, indicating the successful synthesis of AOBC.

Preparation of AuNPs/AOBC Nanohybrids. We have found that the hydroxyl and amidoxime groups on cellulose can act as the reducing agent in the preparation of metal nanoparticles and the amidoxime groups can act as the *in situ* stabilizer for its characteristics of selective chelation of metal ions in our previous work.[21] In this work, AuNPs were synthesized by a one-step approach by heating the mixed suspension of AOBC and $HAuCl_4$ to 110 °C, during which the suspension changed quickly from light yellow to pink purple. The characteristic peak at 524 nm on the UV−vis spectra of the obtained samples comes from the surface plasmon resonance (SPR) band of small AuNPs (Figure S1, Supporting Information).[42] Figure 3 shows the TEM images of AuNPs/AOBC prepared by using AOBC with the amidoxime group content of 16.8 wt %. The obtained AuNPs are spherical with the diameter of 10.6 ± 2.9 nm and distribute equally on the surface of the AOBC nanofibers (Figure 3a−c). High resolution TEM (HRTEM) image of the obtained AuNPs shows the clear lattice with average lattice spacing of 0.23 nm (Figure 3d), which matches the *d*-spacing of the (111) plane of face-

DOI: 10.1021/acsami.5b07150
ACS Appl. Mater. Interfaces 2015, 7, 21717−21726

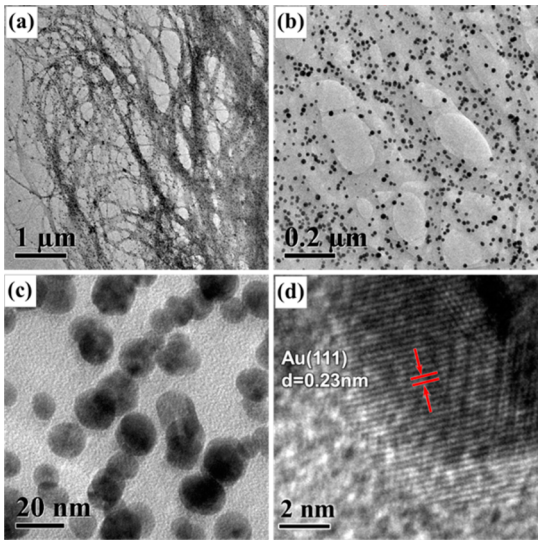

Figure 3. TEM images of AuNPs/AOBC with different magnifications (a–c) and HRTEM image of AuNPs (d).

centered cubic (fcc) Au and confirms the formation of AuNPs crystals.

Figure 4 shows the XRD curves of BC and AuNPs/AOBC. The peaks at 14.3°, 16.7°, and 22.6° correspond to the (1$\bar{1}$0),

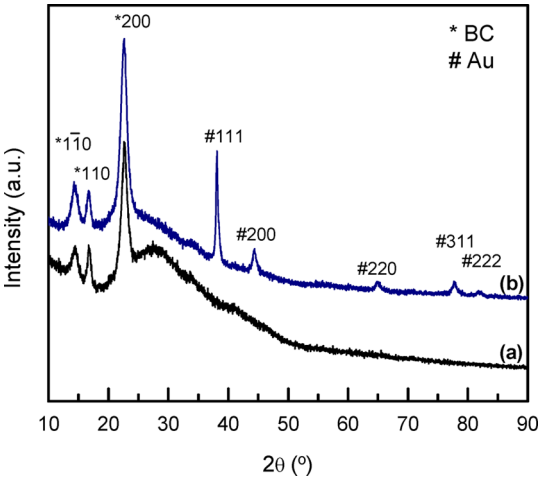

Figure 4. XRD patterns of (a) BC nanofibers and (b) AuNPs/AOBC.

(110), and (200) reflections of crystalline cellulose I, respectively.[43] On the XRD curve of AuNPs/AOBC, additional peaks located at 38.1°, 44.4°, 64.7°, 77.7°, and 81.8° (Figure 4b) appear, corresponding to the diffraction of (111), (200), (220), (311), and (222) planes of fcc Au, respectively.[44] XRD results confirm the success in the synthesis of AuNPs. Meanwhile, it also indicates that the modification and reducing procedures for preparing AuNPs and the presence of AuNPs have no obvious effect on the crystallography of BC.

AOBC samples with different content of amidoxime groups were used for *in situ* synthesis of AuNPs. Figure 5 shows the UV–vis spectra of synthesized AuNPs/AOBC suspensions prepared by using AOBC with different contents of amidoxime groups and the typical TEM images. The absorption peak of the SPR band of AuNPs shifts from 548 to 524 nm with the increase in the amidoxime group content in AOBC (Figure 5a). The color of the final suspensions changes from purple to pink

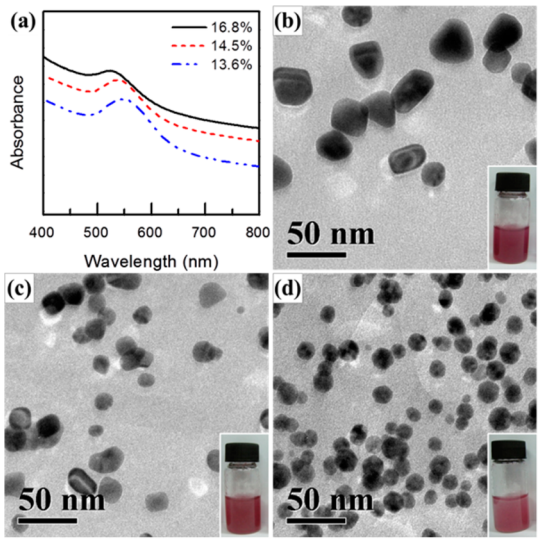

Figure 5. UV–vis spectra (a), and TEM images of AuNPs synthesized by AOBC wih (b) 13.6 wt %, (c) 14.5 wt %, and (d) 16.8 wt % amidoxime groups. Inset images are the photos of the suspension solutions.

purple accordingly (inset photos, Figure 5b–d). TEM observation indicates AuNPs are well distributed on the surface of the AOBC nanofibers without any aggregation (Figure 5b–d). Moreover, the size and shape of AuNPs depend on the content of amidoxime groups used in AOBC. In the case of using AOBC with low amidoxime group content (e.g., 13.6 wt %), the obtained AuNPs are not uniform in size and shape. AuNPs in sphere, triangle, and square can be observed with an average size of 25.8 ± 4.6 nm (Figure 5b). The size of AuNPs is reduced and the morphology simultaneously changes with the increase in amidoxime group content in AOBC. In the case of using AOBC with the amidoxime group content of 16.8 wt %, the AuNPs obtained are mainly spherical with the average size of 10.6 ± 2.9 nm (Figure 5d). This is because the amidoxime groups on the cellulose nanofibers act as nucleation sites on BC surfaces by chelating Au^{3+} ions and reducing them to Au^0. It is reasonable that more nucleation sites on BC surface resulted in AuNPs of smaller size. Moreover, the content of AuNPs in the AuNPs/AOBC also decreases with the increase in the amidoxime group content in AOBC that was used for the preparation of AuNPs, and the particle size frequency distribution of the obtained AuNPs by different contents of amidoxime groups in AOBC (Table 1 and Figure S2). The reason for the decrease in AuNP content with the increase in amidoxime groups on the BC surface is still unclear. One possibility could be the loss of AuNPs during the wash of the resultant AuNPs/AOBC nanohybrids.

Table 1. AuNPs Synthesized by Using AOBC with Different Contents of Amidoxime Groups

samples	W_{Am}[a] (wt %)	AuNPs size[b] (nm)	W_{AuNPs}[c] (mg/g)
AuNPs/AOBC1	13.6	25.8 ± 4.6	19.0
AuNPs/AOBC2	14.5	16.3 ± 4.3	11.6
AuNPs/AOBC3	15.9	13.6 ± 3.0	4.9
AuNPs/AOBC4	16.8	10.6 ± 2.9	4.8

[a]Content of amidoxime groups in AOBC estimated by elemental analysis. [b]Diameter of AuNPs statistically estimated by TEM images. [c]Content of AuNPs in AuNPs/AOBC that measured by ICP analysis.

DOI: 10.1021/acsami.5b07150
ACS Appl. Mater. Interfaces 2015, 7, 21717–21726

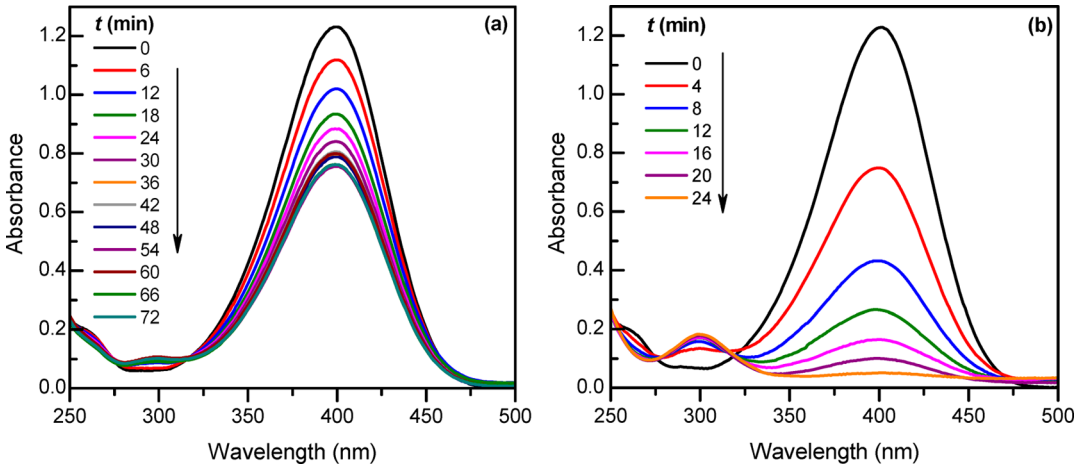

Figure 6. Time dependent UV−vis spectra of the reduction of 4-NP at $NaBH_4$ concentration of (a) 37.5 and (b) 344 mM. The concentrations of 4-NP and AuNPs were 0.30 mM and 0.0286 mg/mL, respectively.

The chemical structure of AOBC during the preparation of AuNPs has been investigated by FTIR. However, the chemical change of AOBC is undetectable by FTIR, which could be due to a small change of AOBC. In the preparation of AuNPs, both hydroxyl and amidoxime groups can take part in the reaction during AuNPs synthesis. It has been proven that the oxidation of cellulose by $Au^{(III)}$ occurred at the hydroxyl groups in AuNPs synthesis by hydrothermal method in the presence of nanocellulose.[19] To clarify the role of amidoxime groups of AOBC in the preparation of AuNPs, polyamidoxime (PAO) was used as a model polymer to synthesize AuNPs by hydrothermal method (details are shown in Supporting Information). By comparing the FTIR spectra of PAO and PAO/AuNPs (Figure S3, Supporting Information), the new bands at 1689 and 1216 cm^{-1} on FTIR spectrum of PAO/AuNPs correspond to —C═O and −C—O− stretching vibrations, respectively. Moreover, the band of —C═N stretching vibration at 1652 cm^{-1} of PAO splits into two peaks (Figure S3, inset, Supporting Information), indicating that amidoxime groups have been partially oxidized into $-CONH_2$ or −COOH groups during AuNPs preparation. All the amidoxime, $-CONH_2$, and −COOH groups in the system have a strong chelation ability and can act as the anchor points to immobilize AuNPs on BC surface through complexion or electrostatic interactions,[39,45,46] which prevent the aggregation of AuNPs.

The interactions between AOBC and AuNPs were investigated by XPS. In the XPS spectra of the Au 4f core of AuNPs/AOBC (Figure S4, Supporting Information), the peaks at the binding energy of 84.3 and 87.9 eV correspond to Au $4f_{7/2}$ and Au $4f_{5/2}$ electrons, respectively.[47] The binding energy of Au 4f core level shifts from 83.8 to 84.3 eV. The shifting of the peaks as compared to the literature value may also be due to the interactions between the deposited AuNPs and AOBC.[48] The XPS spectra of the C 1s, O 1s, and N 1s are shown in Figure S5 (Supporting Information) and the binding energies of the corresponding peaks are listed in Table S2. In AOBC, C 1s, C 1s1, C 1s2, and C 1s3 bond forms, corresponding to **C**−C or **C**−H at 284.8 eV, **C**−OH at 286.3 eV, and O−**C**−O at 287.6, respectively. O 1s contains O 1s1 and O 1s2 bond forms, corresponding to C−**O**H···**O** at 532.3 eV and C−**O**H at 532.9 eV, respectively. The contents of C 1s1 and O 1s1 decrease in AuNPs/AOBC comparing with that in AOBC (Figure S5 and Table S2, Supporting Information), which could be due to the interactions between **C**−H or C−**O**H of AOBC and AuNPs. The N 1s XPS spectra of AOBC can be fitted with two peaks with the binding energies at 399.6 and 400.5 eV (Figure S5c, Supporting Information), corresponding to H_2**N**−C and −C═**N**—OH, respectively. After the preparation and loading of AuNPs, only one peak at 399.6 eV can be observed on the N 1s XPS spectrum of AuNPs/AOBC (Figure S5c′, Supporting Information), confirming that amidoxime groups took part in the reducing reaction and could be changed into H_2**N**—C═O.

Catalytic Activity of AuNPs/AOBC Nanohybrids. The reduction of 4-NP by $NaBH_4$, a standard model reaction for estimating catalytic activity of AuNPs,[28,49,50] was used to evaluate the catalytic properties of AuNPs/AOBC. The catalytic reaction was monitored by UV−vis spectroscopy. The aqueous solution of 4-NP in faint yellow changed into yellow-green with the addition of $NaBH_4$ due to the formation of 4-nitrophenolate ion. The maximum absorption peak of 4-NP aqueous solution located at 317 nm shifted to 400 nm after the addition of $NaBH_4$ (Figure S6a, Supporting Information). Moreover, no obvious changes in the absorbance intensity at 400 nm can be detected within 50 min (Figure S6a, Supporting Information). A similar result can be found for the 4-NP/$NaBH_4$ aqueous solution in the presence of AOBC (Figure S6b, Supporting Information). These results suggest that 4-NP cannot be reduced by $NaBH_4$ or the reduction cannot be detected during the time scale of the experiments. The results confirm that AOBC has no obvious catalytic activity for the reduction of 4-NP by using $NaBH_4$. With the addition of AuNPs/AOBC in 4-NP/$NaBH_4$ aqueous solutions, the color of the reaction solution faded from yellow-green to transparent with time, and small bubbles released continuously from the surface of AuNPs/AOBC, which indicates the occurrence of the reduction reaction in the system. Figure 6 shows the typical time dependent UV−vis spectra of 4-NP/$NaBH_4$ aqueous solutions in the presence of AuNPs/AOBC. At low $NaBH_4$ concentration, e.g., 37.5 mM, the absorbance intensity at 400 nm decreases slowly with reaction time and a new peak at 300 nm appears simultaneously, corresponding to the characteristic absorption of 4-aminophenol (4-AP). The reducing reaction is rather slow and only part of 4-NP can be reduced after 1 h (Figure 6a). With the increase in $NaBH_4$ concentration in the reaction mixture, the absorbance intensity at 400 nm decreases

DOI: 10.1021/acsami.5b07150
ACS Appl. Mater. Interfaces 2015, 7, 21717−21726

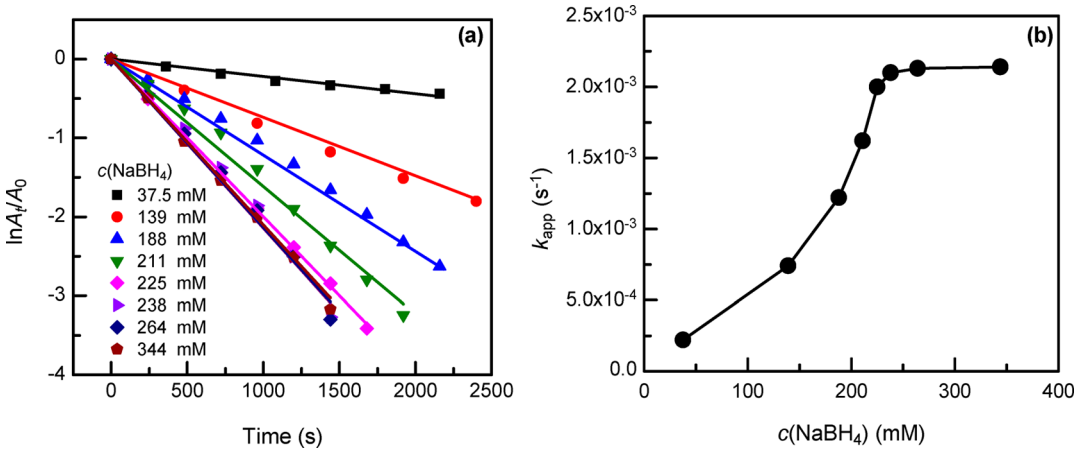

Figure 7. Plot of $\ln(A_t/A_0)$ versus time at different $NaBH_4$ concentration (a) and the reaction rate constant k as a function of $NaBH_4$ concentration (b). Initial concentration of 4-NP in all experiments was kept at 0.30 mM and the content of AuNPs was 0.0286 mg/mL.

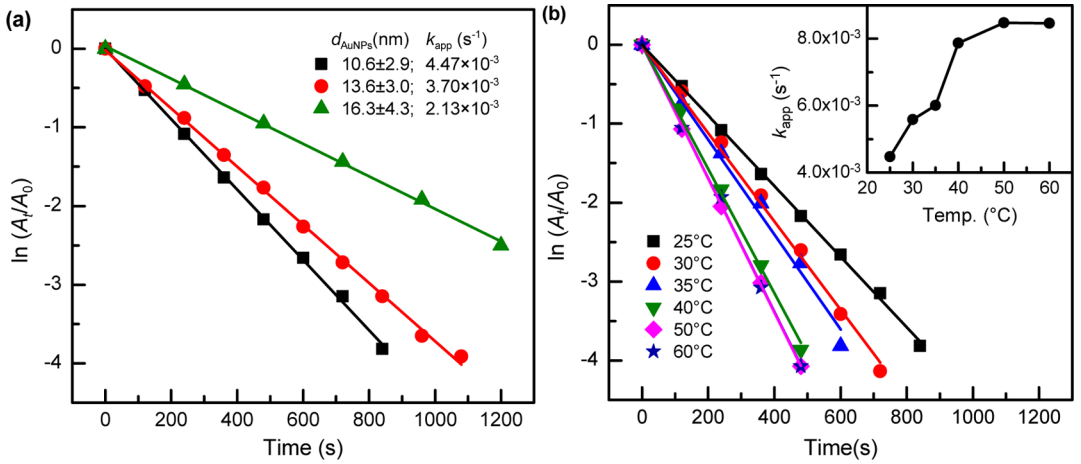

Figure 8. Effect of (a) AuNPs size and (b) temperature on reaction activity of AuNPs/AOBC. Inset figure in (b) is the reaction rate constant k as a function of temperature. Concentrations of 4-NP, $NaBH_4$, and AuNPs in all reaction mixtures were kept at 0.30 mM, 264 mM, and 0.0106 mg/mL, respectively.

much faster (Figure S7, Supporting Information), which indicates the increase in the reaction rate. On the contrary, the reducing reaction is fast at high $NaBH_4$ concentration (e.g., 344 mM) and the 4-NP can be completely reduced within 25 min (Figure 6b).

The reaction kinetics can be depicted by plotting absorbance at 400 nm on the UV−vis spectra of the solutions as a function of reaction time, by which the catalytic activity of AuNPs/AOBC was estimated. Figure 7a shows the plot of $\ln(A_t/A_0)$ versus reaction time, where A_t is the absorbance at reaction time t and A_0 is the initial absorbance. The results indicate that $\ln(A_t/A_0)$ decreases linearly with reaction time, which is consistent with the pseudo-first-order kinetics of 4-NP reduction by $NaBH_4$ using AuNPs as catalyst.[49] The apparent reaction rate constant k_{app} (s^{-1}) was estimated by the linear fitting of the experimental results as shown in Figure 7a and k_{app} as a function of $NaBH_4$ concentration is shown in Figure 7b. The results indicate that k_{app} depends on $NaBH_4$ concentration in the system. At $NaBH_4$ concentration below 238 mM, k_{app} increases with the increase in $NaBH_4$ concentration. At $NaBH_4$ concentration above 238 mM, k_{app} is independent of $NaBH_4$ concentration. Suitable stoichiometric ratio of 4-NP and $NaBH_4$ that ensures completely reduction of 4-NP should be selected in practical applications.

The catalytic activity of AuNPs/AOBC in the reducing reaction of 4-NP also depends on AuNPs size. The time dependent UV−vis spectra of the reducing reaction of 4-NP catalyzed by AuNPs/AOBC with different size of AuNPs are shown in Figure S8 (Supporting Information). The results indicate that all the reduction reaction can be finished within 25 min. Especially, catalytic reduction reaction using the smallest AuNPs (10.6 ± 2.9 nm) is the fastest, in which the reduction reaction can be finished within 14 min (Figure S8a, Supporting Information). Figure 8a shows the $\ln(A_t/A_0)$ versus reaction time of AuNPs/AOBC with different AuNPs size. The apparent reaction rate constant k_{app} of AuNPs/AOBC decreases with the increase in AuNPs size, e.g., 4.47 × 10^{-3}, 3.70 × 10^{-3}, and 2.13 × 10^{-3} s^{-1} for AuNPs/AOBC with the AuNPs size of 10.6 ± 2.9, 13.6 ± 3.0, and 16.3 ± 4.3 nm, respectively. Moreover, the values of the apparent reaction rate constant in this work are at the same level as those in the literature (Table 1). The temperature dependence of catalytic activity of AuNPs/AOBC was also investigated. Figure 8b shows the $\ln(A_t/A_0)$ versus reaction time of the AuNPs/AOBC at different temperature. The UV−vis spectra are provided in Figure S9. The results indicate that the catalytic reduction of 4-NP by $NaBH_4$ in the presence of AuNPs/AOBC becomes faster with the increase in the temperature, which can be confirmed by the increase in k_{app}

DOI: 10.1021/acsami.5b07150
ACS Appl. Mater. Interfaces 2015, 7, 21717−21726

Table 2. Reduction of 4-NP over Au Nano-Catalysts

support	T^a (K)	AuNPs size (nm)	$NaBH_4$/4-NP/Au (mole ratio)	$k_{app}{}^b$ (s^{-1})	$TOF_a{}^c$ (h^{-1})	refs
PMMA	295	6.9	22500/15/1	7.2×10^{-3}	88.6	49
PDMAEMA-PS	298	4.2	28/0.14/1	3.2×10^{-3}	0.7	54
PNIPAP-*b*-P4VP	298	3.3	167/5/1	1.5×10^{-3}	15.5	50
CNs	298	10−30	9720/30/1	2.1×10^{-3}	109	19
Chitosan	303	3.1	20/6/1	1.2×10^{-2}	50.4	55
α-CD	298	20	250/6/1	4.7×10^{-3}	34.0	34
None	[d]	100	2/0.02/1	1.2×10^{-2}	0.4	56
Poly(DVB-*co*-AA)	298	9.1−12.4	9800/267/1	6.0×10^{-3}	222	57
CSNFs	298	5	150000/150/1	5.9×10^{-3}	560	28
PDDA/NCC	298	3.09 ± 0.15	36585/37/1	5.1×10^{-3}	212	26
AOBC-1	298	16.3 ± 4.3	1034/104/1	2.1×10^{-3}	260	This work
AOBC-2	298	13.6 ± 3.0	235714/270/1	3.7×10^{-3}	899	
AOBC-3	298	10.6 ± 2.9	244444/280/1	4.5×10^{-3}	1198	

[a]Reaction temperature. [b]Pseudo-first-order reaction rate constant per total Au content. [c]TOF_a estimated using the data in corresponding references. [d]No data available.

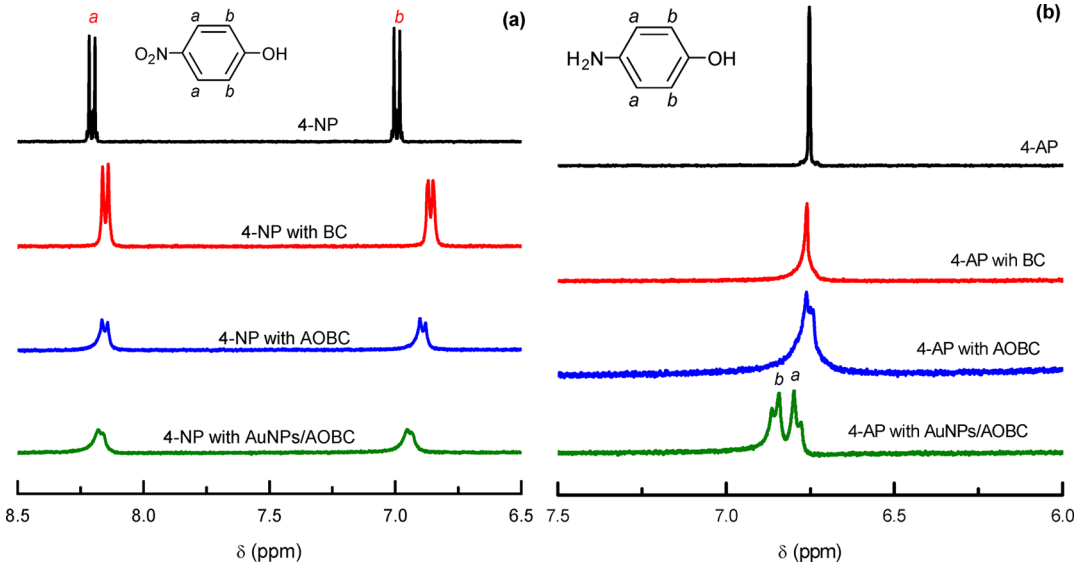

Figure 9. Typical ^1H NMR spectra of (a) 4-NP and (b) 4-AP in D_2O and in the presence of BC, AOBC, and AuNPs/AOBC.

with the increasing temperature. The activation energy for the catalytic reaction was found to be 20.84 kJ·mol^{-1} for AuNPs with the size of 10.6 nm. Meanwhile, k_{app} reached the biggest value at 50 °C (Figure 8b, inset). The heterogeneous catalytic reactions generally follow the Sabatier principle, the key molecular principle of catalysis.[51] The substrate molecules have to adsorb to the catalyst and become activated, and the product molecules have to desorb. According to this principle, the rate of catalytic reaction has a maximum when the rate of activation and the rate of product desorption balance. In this work, the balance could be around 50 °C, at which the maximum in the volcano plot was reached.[51]

Some active sites of the supported or stabilized catalysts are inevitably covered by the supports or stabilizers, as for the active sites of AuNPs in the AuNPs/AOBC nanohybrids in present work. In such cases, the catalytic efficiency can be estimated by apparent turnover frequency (TOF_a) defined as[19,52,53]

$$TOF_a = n_p/n_c t \quad (1)$$

where n_p and n_c are the moles of product molecules during time t and the catalyst, respectively. Herein, n_c is the number of Au atoms in the AuNPs/AOBC, which was estimated by the content of Au in the samples that was measured by using ICP analysis. TOF_a values of the AuNPs/AOBC in this work and those in the literature are listed in Table 2. The results indicate that TOF_a increases with the increase in the size of AuNPs. The highest TOF_a value of AuNPs/AOBC in this work is 1190 h^{-1}, much higher than those in the literature (Table 2). For clarifying the higher TOF_a in this work, we plotted the TOF_a as a function of the mole ratio of 4-NP to gold atoms, [4-NP]/[Au], in the reaction systems that are listed in Table 2. The results indicated that TOF_a increases, possibly linearly, with increasing [4-NP]/[Au] (Figure S10, Supporting Information), which can lead to the conclusion that the higher TOF_a could be generally due to the higher mole ratio of 4-NP to gold atoms in the reaction system.

It should be noted that the size of the AuNPs in this is larger than most of the AuNPs in the literature that are listed in Table 2. It is generally known that larger AuNPs should have fewer active sites and lower catalytic activity. However, the apparent reaction rate constant k_{app} of AuNPs/AOBC is surprisingly at the same level as those of AuNPs with smaller size (Table 2). The high catalytic activity of the AuNPs/AOBC nanohybrids

DOI: 10.1021/acsami.5b07150
ACS Appl. Mater. Interfaces 2015, 7, 21717−21726

prepared in this work is expected because the AuNPs synthesized are well dispersed and stabilized on the AOBC nanofiber surface, which ensures the effective contact of the active sites with the reactants. The specific surface area of the AuNPs/AOBC prepared from AOBC with different contents of amidoxime groups were measured by BET and the results are listed in Table S3 (Supporting Information). The results indicate that the specific surface area of AuNPs/AOBC is quite low, about 38−50 $m^2 \cdot s^{-1}$. Therefore, the high catalytic activity of AuNPs/AOBC could not be attributed to the high specific surface area, or the high content of the active sites, of the nanohybrids.

In order to clarify the origins of the high catalytic activity of the AuNPs/AOBC on the reduction of 4-NP, the status of 4-NP and 4-AP in D_2O solutions was investigated by using ^1H NMR (Figure 9). The results indicate that 4-NP molecules are well solvated in deuterated water (Figure 9a). With the addition of BC, the characteristic peaks of 4-NP become slightly wider and weaker, suggesting there are interactions between 4-NP and BC. With the addition of AOBC, the characteristic peaks of 4-NP become even weaker and wider, indicating that there are strong interactions between 4-NP molecules and AOBC surface. In the case of adding AuNPs/AOBC, the characteristic peaks of 4-NP are wider and weaker with the disappearance of the peak split, which suggests that 4-NP molecules are adsorbed on the surface of the AuNPs/AOBC, especially on the AuNPs surface compared with the ^1H NMR spectrum in the presence of AOBC (Figure 9a). The good affinity of 4-NP on the surface of AuNPs and AOBC can effectively promote the catalytic efficiency of AuNPs on the reducing reaction. Figure 9b shows the ^1H NMR spectra of 4-AP, the reduced product of 4-NP, in D_2O with different additives. The sharp peak of 4-AP in D_2O could be due to the intramolecular interaction of 4-AP or the intermolecular interaction between 4-AP and D_2O. With the addition of AOBC and AuNPs/AOBC, the resonance signals of 4-AP split, indicating the enhancement of the solvation of 4-AP molecules in the system. Good solvation of 4-AP could promote the solubility of 4-AP in the system and 4-AP molecules are preferred to leave the surfaces of AuNPs and AOBC. The results above suggest that the active sites of the AuNPs/AOBC could be automatically refreshed during the catalysis of the reducing reaction of 4-NP with $NaBH_4$, which can synergistically provide the excellent catalytic activity of the AuNPs/AOBC prepared in this work. On the other hand, the amidoxime groups in the AuNPs/AOBC have the fused features of amide, oxime, amidine, and hydroxamic groups,[21,36] which helped the electron transfer process between the BH_4^- and nitro compounds.[14,58−60] Therefore, the synergistic effects of the affinity between the AuNPs/AOBC and the 4-NP, 4-AP, and BH_4^- in the system offer the high catalytic activity of the AuNPs/AOBC nanohybrids prepared in this work. The mechanism for enhancing the catalytic activity of catalysts could be extended for designing other catalysts for special applications.

To evaluate the practical applications of AuNPs/AOBC as the catalyst, a glass tube column with an inner diameter of 7.5 mm and a length of 300 mm was filled with the AuNPs/AOBC prepared in this work (Figure S11, Supporting Information). AuNPs/AOBC suspension (3 mL) containing 0.0857 mg AuNPs in the size of 16.3 ± 4.3 nm was mixed with a 60 mL paste prepared by beating 20.2 g filter paper in 700 mL water. The mixture was mixed with sea sand (particle size of 0.65−0.85 mm). The column was filled by wet method with about 18 mm pure sea sand at both bottom and top end of the column. The sea sand at the bottom of the column was stopped by filling cotton. The column was first filled with water by using a peristaltic pump (HL-2S series, Shanghai, China). For continuous reduction experiments, the mixed solution with the 4-NP (0.30 mM) and $NaBH_4$ (238 mM) under stirring was continuously fed into the column at a flow rate of 0.75 mL min^{-1} (Figure S11, Supporting Information). The reduction 4-NP by $NaBH_4$ under the catalysis of AuNPs/AOBC nanohybrid was monitored by the UV−vis spectra of the eluent collected in the beaker. The disappearance of the absorbance at 400 nm in the UV−vis spectra of the eluent confirms the complete reduction of the 4-NP (Figure S11b, Supporting Information). After 3500 times of the 4-NP per unit mass of AuNPs contained in the AuNPs/AOBC have been reduced, the column is still running well. The column has been running for two months and it still works well without any loss in catalytic activity. The results confirm that the AuNPs/AOBC prepared in the present work is an excellent catalyst for the reduction of 4-NP by $NaBH_4$. The applications in other fields or for the catalysis of other possible chemical reaction are promising. The method can be extended for any other cellulose materials, such as cellulose fibers, membranes, and nanocrystal cellulose.

CONCLUSIONS

Amidoxime surface functionalized bacterial cellulose (AOBC) was successfully synthesized without affecting the morphology of BC. The content of amidoxime groups in AOBC can be adjusted by varying the reaction parameters. AOBC with different contents of amidoxime groups were used as the reducing agent and carrier for preparing AuNPs. It was found that a higher content of amidoxime group in AOBC is beneficial for the preparation of AuNPs with smaller and more uniform size. AuNPs distributed homogeneously on the surface of BC. The resultant AuNPs/AOBC nanohybrids can be used as the excellent catalyst in the reduction of 4-NP by $NaBH_4$. The catalytic activity of AuNPs/AOBC depended on the $NaBH_4$ concentration and temperature of the reaction mixture, as well as the AuNP size. The catalytic activity first increased with the increasing $NaBH_4$ concentration and the temperature, and then leveled off at the $NaBH_4$ concentration above 238 mM and temperature above 50 °C. Moreover, AuNPs with smaller size have higher catalytic activity. The higher catalytic activity of the AuNPs/AOBC come from the high affinity of 4-NP to the surface of AOBC and AuNPs and the good solvation of the reducing product 4-AP. A column containing AuNPs/AOBC has been filled for the continuous catalysis of the reduction of 4-NP using $NaBH_4$. The column worked well without detection of 4-NP in the eluent for more than two months. This work provides a green approach for the preparation of an excellent catalyst based on bacterial cellulose stabilized AuNPs.

ASSOCIATED CONTENT

Supporting Information

The Supporting Information is available free of charge on the ACS Publications website at DOI: 10.1021/acsami.5b07150.

Time dependent UV−vis spectra of the reduction of 4-NP by $NaBH_4$ using AuNPs/AOBC as the catalyst (PDF)

DOI: 10.1021/acsami.5b07150
ACS Appl. Mater. Interfaces 2015, 7, 21717−21726

AUTHOR INFORMATION

Corresponding Authors

*E-mail: hlkang@iccas.ac.cn.
*E-mail: ymgong@dlpu.edu.cn.
*E-mail: rgliu@iccas.ac.cn. Tel. and Fax: +86-10-82618573.

Notes

The authors declare no competing financial interest.

ACKNOWLEDGMENTS

This work was supported by National Natural Science Foundation of China (21274154, 51473174, 51103017, and 51003108), the Cooperative Innovation Program of Sate Key Laboratory of Polymer Physics and Chemistry (PPCL-2014-CX-1) and the opening topic fund of Beijing Key laboratory of Organic Material Testing Technology and Quality Evaluation (201502004).

REFERENCES

(1) Daniel, M. C.; Astruc, D. Gold Nanoparticles: Assembly, Supramolecular Chemistry, Quantum-Size-Related Properties, and Applications toward Biology, Catalysis, and Nanotechnology. *Chem. Rev.* **2004**, *104*, 293−346.

(2) Jain, P. K.; Huang, X. H.; El-Sayed, I. H.; El-Sayed, M. A. Noble Metals on the Nanoscale: Optical and Photothermal Properties and Some Applications in Imaging, Sensing, Biology, and Medicine. *Acc. Chem. Res.* **2008**, *41*, 1578−1586.

(3) Hu, M.; Chen, J. Y.; Li, Z. Y.; Au, L.; Hartland, G. V.; Li, X. D.; Marquez, M.; Xia, Y. N. Gold Nanostructures: Engineering Their Plasmonic Properties for Biomedical Applications. *Chem. Soc. Rev.* **2006**, *35*, 1084−1094.

(4) Layek, K.; Chakravarti, R.; Kantam, M. L.; Maheswaran, H.; Vinu, A. Nanocrystalline Magnesium Oxide Stabilized Gold Nanoparticles: An Advanced Nanotechnology Based Recyclable Heterogeneous Catalyst Platform for the One-Pot Synthesis of Propargylamines. *Green Chem.* **2011**, *13*, 2878−2887.

(5) Oliveira, R. L.; Kiyohara, P. K.; Rossi, L. M. Clean Preparation of Methyl Esters in One-Step Oxidative Esterification of Primary Alcohols Catalyzed by Supported Gold Nanoparticles. *Green Chem.* **2009**, *11*, 1366−1370.

(6) Tan, X. S.; Deng, W. P.; Liu, M.; Zhang, Q. H.; Wang, Y. Carbon Nanotube-Supported Gold Nanoparticles as Efficient Catalysts for Selective Oxidation of Cellobiose into Gluconic Acid in Aqueous Medium. *Chem. Commun.* **2009**, 7179−7181.

(7) Kundu, S.; Jayachandran, M. The Self-Assembling of DNA-Templated Au Nanoparticles into Nanowires and Their Enhanced Sers and Catalytic Applications. *RSC Adv.* **2013**, *3*, 16486−16498.

(8) Chen, J. Y.; Wiley, B. J.; Xia, Y. N. One-Dimensional Nanostructures of Metals: Large-Scale Synthesis and Some Potential Applications. *Langmuir* **2007**, *23*, 4120−4129.

(9) Murphy, C. J.; Gole, A. M.; Hunyadi, S. E.; Orendorff, C. J. One-Dimensional Colloidal Gold and Silver Nanostructures. *Inorg. Chem.* **2006**, *45*, 7544−7554.

(10) Murphy, C. J.; San, T. K.; Gole, A. M.; Orendorff, C. J.; Gao, J. X.; Gou, L.; Hunyadi, S. E.; Li, T. Anisotropic Metal Nanoparticles: Synthesis, Assembly, and Optical Applications. *J. Phys. Chem. B* **2005**, *109*, 13857−13870.

(11) Grzelczak, M.; Perez-Juste, J.; Mulvaney, P.; Liz-Marzan, L. M. Shape Control in Gold Nanoparticle Synthesis. *Chem. Soc. Rev.* **2008**, *37*, 1783−1791.

(12) Xia, Y. N.; Xiong, Y. J.; Lim, B.; Skrabalak, S. E. Shape-Controlled Synthesis of Metal Nanocrystals: Simple Chemistry Meets Complex Physics? *Angew. Chem., Int. Ed.* **2009**, *48*, 60−103.

(13) Hermes, J. P.; Sander, F.; Peterle, T.; Urbani, R.; Pfohl, T.; Thompson, D.; Mayor, M. Gold Nanoparticles Stabilized by Thioether Dendrimers. *Chem. - Eur. J.* **2011**, *17*, 13473−13481.

(14) Kundu, S.; Wang, K.; Liang, H. Size-Selective Synthesis and Catalytic Application of Polyelectrolyte Encapsulated Gold Nanoparticles Using Microwave Irradiation. *J. Phys. Chem. C* **2009**, *113*, 5157−5163.

(15) Sekhar, A. C. S.; Meera, C. J.; Ziyad, K. V.; Gopinath, C. S.; Vinod, C. P. Synthesis and Catalytic Activity of Monodisperse Gold-Mesoporous Silica Core-Shell Nanocatalysts. *Catal. Sci. Technol.* **2013**, *3*, 1190−1193.

(16) Wang, S.; Zhang, M.; Zhang, W. Yolk−Shell Catalyst of Single Au Nanoparticle Encapsulated within Hollow Mesoporous Silica Microspheres. *ACS Catal.* **2011**, *1*, 207−211.

(17) Ishida, T.; Haruta, M. Gold Catalysts: Towards Sustainable Chemistry. *Angew. Chem., Int. Ed.* **2007**, *46*, 7154−7156.

(18) Laudenslager, M. J.; Schiffman, J. D.; Schauer, C. L. Carboxymethyl Chitosan as a Matrix Material for Platinum, Gold, and Silver Nanoparticles. *Biomacromolecules* **2008**, *9*, 2682−2685.

(19) Wu, X. D.; Lu, C. H.; Zhou, Z. H.; Yuan, G. P.; Xiong, R.; Zhang, X. X. Green Synthesis and Formation Mechanism of Cellulose Nanocrystal-Supported Gold Nanoparticles with Enhanced Catalytic Performance. *Environ. Sci.: Nano* **2014**, *1*, 71−79.

(20) Tan, J. J.; Liu, R. G.; Wang, W.; Liu, W. Y.; Tian, Y.; Wu, M.; Huang, Y. Controllable Aggregation and Reversible pH Sensitivity of AuNPs Regulated by Carboxymethyl Cellulose. *Langmuir* **2010**, *26*, 2093−2098.

(21) Li, W. W.; Liu, R. G.; Kang, H. L.; Sun, Y. M.; Dong, F. Y.; Huang, Y. Synthesis of Amidoxime Functionalized Cellulose Derivatives as a Reducing Agent and Stabilizer for Preparing Gold Nanoparticles. *Polym. Chem.* **2013**, *4*, 2556−2563.

(22) Kang, H. L.; Liu, R. G.; Huang, Y. Cellulose Derivatives and Graft Copolymers as Blocks for Functional Materials. *Polym. Int.* **2013**, *62*, 338−344.

(23) Kang, H. L.; Liu, R. G.; Huang, Y. Graft Modification of Cellulose: Methods, Properties and Applications. *Polymer* **2015**, *70*, A1−A16.

(24) Niu, T.; Xu, J. B.; Xiao, W.; Huang, J. G. Cellulose-Based Catalytic Membranes Fabricated by Deposition of Gold Nanoparticles on Natural Cellulose Nanofibres. *RSC Adv.* **2014**, *4*, 4901−4904.

(25) Zhang, T. J.; Wang, W.; Zhang, D. Y.; Zhang, X. X.; Ma, Y. R.; Zhou, Y. L.; Qi, L. M. Biotemplated Synthesis of Gold Nanoparticle-Bacteria Cellulose Nanofiber Nanocomposites and Their Application in Biosensing. *Adv. Funct. Mater.* **2010**, *20*, 1152−1160.

(26) Lam, E.; Hrapovic, S.; Majid, E.; Chong, J. H.; Luong, J. H. Catalysis Using Gold Nanoparticles Decorated on Nanocrystalline Cellulose. *Nanoscale* **2012**, *4*, 997−1002.

(27) Ashraf, S.; Saif-ur-Rehman; Sher, F.; Khalid, Z. M.; Mehmood, M.; Hussain, I. Synthesis of Cellulose−Metal Nanoparticle Composites: Development and Comparison of Different Protocols. *Cellulose* **2014**, *21*, 395−405.

(28) Koga, H.; Tokunaga, E.; Hidaka, M.; Umemura, Y.; Saito, T.; Isogai, A.; Kitaoka, T. Topochemical Synthesis and Catalysis of Metal Nanoparticles Exposed on Crystalline Cellulose Nanofibers. *Chem. Commun.* **2010**, *46*, 8567−8569.

(29) Dong, H.; Hinestroza, J. P. Metal Nanoparticles on Natural Cellulose Fibers: Electrostatic Assembly and in Situ Synthesis. *ACS Appl. Mater. Interfaces* **2009**, *1*, 797−803.

(30) He, J. H.; Kunitake, T.; Nakao, A. Facile in Situ Synthesis of Noble Metal Nanoparticles in Porous Cellulose Fibers. *Chem. Mater.* **2003**, *15*, 4401−4406.

(31) Cai, J.; Kimura, S.; Wada, M.; Kuga, S. Nanoporous Cellulose as Metal Nanoparticles Support. *Biomacromolecules* **2009**, *10*, 87−94.

(32) Mahmoud, K. A.; Male, K. B.; Hrapovic, S.; Luong, J. H. T. Cellulose Nanocrystal/Gold Nanoparticle Composite as a Matrix for Enzyme Immobilization. *ACS Appl. Mater. Interfaces* **2009**, *1*, 1383−1386.

(33) Azetsu, A.; Koga, H.; Yuan, L. Y.; Kitaoka, T. Direct Synthesis of Gold Nanocatalysts on Tempo-Oxidized Pulp Paper Containing Aldehyde Groups. *BioResources* **2013**, *8*, 3706−3717.

(34) Huang, T.; Meng, F.; Qi, L. M. Facile Synthesis and One-Dimensional Assembly of Cyclodextrin-Capped Gold Nanoparticles and Their Applications in Catalysis and Surface-Enhanced Raman Scattering. *J. Phys. Chem. C* **2009**, *113*, 13636−13642.

DOI: 10.1021/acsami.5b07150
ACS Appl. Mater. Interfaces 2015, 7, 21717−21726

(35) Lu, W.; Ning, R.; Qin, X.; Zhang, Y.; Chang, G.; Liu, S.; Luo, Y.; Sun, X. Synthesis of Au Nanoparticles Decorated Graphene Oxide Nanosheets: Noncovalent Functionalization by Tween 20 in Situ Reduction of Aqueous Chloroaurate Ions for Hydrazine Detection and Catalytic Reduction of 4-Nitrophenol. *J. Hazard. Mater.* **2011**, *197*, 320−326.
(36) Cao, C.; Kang, H. L.; Che, N.; Liu, Z. J.; Li, P. P.; Zhang, C.; Li, W. W.; Liu, R. G.; Huang, Y. Wool Graft Polyacrylamidoxime as the Adsorbent for Both Cationic and Anionic Toxic Ions from Aqueous Solutions. *RSC Adv.* **2014**, *4*, 60609−60616.
(37) Klemm, D.; Schumann, D.; Udhardt, U.; Marsch, S. Bacterial Synthesized Cellulose - Artificial Blood Vessels for Microsurgery. *Prog. Polym. Sci.* **2001**, *26*, 1561−1603.
(38) Svensson, A.; Nicklasson, E.; Harrah, T.; Panilaitis, B.; Kaplan, D. L.; Brittberg, M.; Gatenholm, P. Bacterial Cellulose as a Potential Scaffold for Tissue Engineering of Cartilage. *Biomaterials* **2005**, *26*, 419−431.
(39) Chen, S. Y.; Shen, W.; Yu, F.; Hu, W. L.; Wang, H. P. Preparation of Amidoximated Bacterial Cellulose and Its Adsorption Mechanism for Cu^{2+} and Pb^{2+}. *J. Appl. Polym. Sci.* **2010**, *117*, 8−15.
(40) Shen, W.; Chen, S. Y.; Shi, S. K.; Li, X.; Zhang, X.; Hu, W. L.; Wang, H. P. Adsorption of Cu(II) and Pb(II) onto Diethylenetriamine-Bacterial Cellulose. *Carbohydr. Polym.* **2009**, *75*, 110−114.
(41) de Santa Maria, L. C.; Santos, A. L. C.; Oliveira, P. C.; Barud, H. S.; Messaddeq, Y.; Ribeiro, S. J. L. Synthesis and Characterization of Silver Nanoparticles Impregnated into Bacterial Cellulose. *Mater. Lett.* **2009**, *63*, 797−799.
(42) Burda, C.; Chen, X. B.; Narayanan, R.; El-Sayed, M. A. Chemistry and Properties of Nanocrystals of Different Shapes. *Chem. Rev.* **2005**, *105*, 1025−1102.
(43) Tokoh, C.; Takabe, K.; Fujita, M.; Saiki, H. Cellulose Synthesized by Acetobacter Xylinum in the Presence of Acetyl Glucomannan. *Cellulose* **1998**, *5*, 249−261.
(44) Li, Z. G.; Friedrich, A.; Taubert, A. Gold Microcrystal Synthesis Via Reduction of Haucl4 by Cellulose in the Ionic Liquid 1-Butyl-3-Methyl Imidazolium Chloride. *J. Mater. Chem.* **2008**, *18*, 1008−1014.
(45) Bera, R. K.; Baral, M.; Sahoo, S. K.; Kanungo, B. K. Spectroscopic, Potentiometric and Theoretical Studies of Novel Imino-Phenolate Chelators for Fe(III). *Spectrochim. Acta, Part A* **2015**, *134*, 165−172.
(46) Miller, D. J.; Sun, L.; Walzak, M. J.; McIntyre, N. S.; Chvedov, D.; Rosenfeld, A. Static Sims Studies of Fatty Alcohols, Amines and Esters on Gold and Aluminium-Magnesium Alloy Surfaces. *Surf. Interface Anal.* **2005**, *37*, 499−508.
(47) Panigrahi, S.; Basu, S.; Praharaj, S.; Pande, S.; Jana, S.; Pal, A.; Ghosh, S. K.; Pal, T. Synthesis and Size-Selective Catalysis by Supported Gold Nanoparticles: Study on Heterogeneous and Homogeneous Catalytic Process. *J. Phys. Chem. C* **2007**, *111*, 4596−4605.
(48) Guczi, L.; Peto, G.; Beck, A.; Frey, K.; Geszti, O.; Molnar, G.; Daroczi, C. Gold Nanoparticles Deposited on Sio2/Si(100): Correlation between Size, Electron Structure, and Activity in Co Oxidation. *J. Am. Chem. Soc.* **2003**, *125*, 4332−4337.
(49) Kuroda, K.; Ishida, T.; Haruta, M. Reduction of 4-Nitrophenol to 4-Aminophenol over Au Nanoparticles Deposited on Pmma. *J. Mol. Catal. A: Chem.* **2009**, *298*, 7−11.
(50) Wang, Y.; Wei, G. W.; Zhang, W. Q.; Jiang, X. W.; Zheng, P. W.; Shi, L. Q.; Dong, A. J. Responsive Catalysis of Thermoresponsive Micelle-Supported Gold Nanoparticles. *J. Mol. Catal. A: Chem.* **2007**, *266*, 233−238.
(51) van Santen, R. A. Molecular Catalytic Kinetics Concepts. In *Novel Concepts in Catalysis and Chemical Reactors: Improving the Efficiency for the Future*; Cybulski, A., Moulijn, J. A., Stankiewicz, A., Eds.; WILEY-VCH Verlag GmbH & Co.: Weinheim, 2010; pp 1−30.
(52) Azevedo, A. M.; Cabral, J. M. S.; Gibson, T. D.; Fonseca, L. P. Operation and Performance of Analytical Packed-Bed Reactors with an Immobilised Alcohol Oxidase. *J. Mol. Catal. B: Enzym.* **2004**, *28*, 45−53.
(53) Boudart, M. Turnover Rates in Heterogeneous Catalysis. *Chem. Rev.* **1995**, *95*, 661−666.
(54) Zhang, M.; Liu, L.; Wu, C.; Fu, G.; Zhao, H.; He, B. Synthesis, Characterization and Application of Well-Defined Environmentally Responsive Polymer Brushes on the Surface of Colloid Particles. *Polymer* **2007**, *48*, 1989−1997.
(55) Chang, Y. C.; Chen, D. H. Catalytic Reduction of 4-Nitrophenol by Magnetically Recoverable Au Nanocatalyst. *J. Hazard. Mater.* **2009**, *165*, 664−669.
(56) Rashid, M. H.; Mandal, T. K. Templateless Synthesis of Polygonal Gold Nanoparticles: An Unsupported and Reusable Catalyst with Superior Activity. *Adv. Funct. Mater.* **2008**, *18*, 2261−2271.
(57) Liu, W.; Yang, X. L.; Huang, W. Q. Catalytic Properties of Carboxylic Acid Functionalized-Polymer Microsphere-Stabilized Gold Metallic Colloids. *J. Colloid Interface Sci.* **2006**, *304*, 160−165.
(58) Nithiyanantham, U.; Ede, S. R.; Kundu, S. Self-Assembled Wire-Like and Honeycomb-Like Osmium Nanoclusters (Ncs) in DNA with Pronounced Catalytic and Sers Activities. *J. Mater. Chem. C* **2014**, *2*, 3782−3794.
(59) Kundu, S.; Wang, K.; Liang, H. Photochemical Generation of Catalytically Active Shape Selective Rhodium Nanocubes. *J. Phys. Chem. C* **2009**, *113*, 18570−18577.
(60) Kundu, S.; Lau, S.; Liang, H. Shape-Controlled Catalysis by Cetyltrimethylammonium Bromide Terminated Gold Nanospheres, Nanorods, and Nanoprisms. *J. Phys. Chem. C* **2009**, *113*, 5150−5156.

DOI: 10.1021/acsami.5b07150
ACS Appl. Mater. Interfaces 2015, 7, 21717−21726